Monthly Notices
of the
ROYAL ASTRONOMICAL SOCIETY

Mon. Not. R. Astron. Soc. **401,** 2715–2721 (2010) doi:10.1111/j.1365-2966.2009.15856.x

The rise of the C IV mass density at $z < 2.5$⋆

Valentina D'Odorico,[1]† Francesco Calura,[1] Stefano Cristiani[1,2] and Matteo Viel[1,2]

[1]*INAF-OATS, Via Tiepolo 11, 34143 Trieste, Italy*
[2]*INFN/National Institute of Nuclear Physics, via Valerio 2, 34127 Trieste, Italy*

Accepted 2009 October 12. Received 2009 October 12; in original form 2009 June 27

ABSTRACT

The cosmic evolution of the metal content of the intergalactic medium puts stringent constraints on the properties of galactic outflows and on the nature of UV background. In this paper, we present a new measure of the redshift evolution of the mass density of C IV, $\Omega_{\rm C\,IV}$, in the interval $1.5 \lesssim z \lesssim 4$ based on a sample of more than 1500 C IV lines with column densities $10^{12} \lesssim N({\rm C\,IV}) \lesssim 10^{15}\,{\rm cm}^{-2}$. This sample more than doubles the absorption redshift path covered in the range $z < 2.5$ by previous samples. The result shows a significant increase of $\Omega_{\rm C\,IV}$ towards the lower redshifts at variance with the previously pictured constant behaviour.

Key words: intergalactic medium – quasars: absorption lines – cosmology: observations.

1 INTRODUCTION

The cosmological mass density of C IV, $\Omega_{\rm C\,IV}$, observed as a function of redshift is a fundamental quantity closely related to the metal enrichment of the intergalactic medium (IGM). Its apparent lack of evolution in the redshift interval $z \simeq [1.5, 5]$ (Songaila 2001, hereafter S01; Pettini et al. 2003; Boksenberg, Sargent & Rauch 2003, hereafter BSR03) is puzzling since both the physical conditions of the IGM and the properties of the ionizing background are thought to evolve between these epochs.

Remarkable efforts have been made in recent years to extend the measure of $\Omega_{\rm C\,IV}$ to redshift larger than 5 (Ryan-Weber, Pettini & Madau 2006; Simcoe 2006) where a decrease of the star formation rate density is observed (Bunker et al. 2006). If $\Omega_{\rm C\,IV}$ is dominated by the metals produced *in situ* by the observed star-forming galaxies, we would expect a decrease of its value at those redshifts. Vice versa, the value of $\Omega_{\rm C\,IV}$ could remain constant if it reflects the metallicity of a diffuse medium pre-enriched at very high redshift. It should be noted, however, that this is a simplified scenario since, as redshift increases, the observed C IV absorptions likely trace gas in structures of decreasing overdensity and also the ionizing spectrum evolves in shape and intensity. As a consequence, the behaviour of $\Omega_{\rm C\,IV}$ could be different from that of $\Omega_{\rm C}$ and of the mean IGM metallicity (see e.g. Schaye et al. 2003).

The most recent measurements of C IV absorptions in spectra of quasi-stellar objects (QSOs) at $z \sim 6$ seem to indicate a downturn in the C IV mass density at $z > 5$ (Becker, Rauch & Sargent 2009; Ryan-Weber et al. 2009), though based only on three detected C IV lines.

At redshift $z \lesssim 4.5$, a fundamental measurement of $\Omega_{\rm C\,IV}$ has been carried out by S01. However, the redshift interval $1.5 < z < 2$ is poorly sampled by the considered QSO spectra. A more uniform redshift coverage is provided by the sample of BSR03 although with fewer QSO spectra. Both analyses are consistent with a constant behaviour of $\Omega_{\rm C\,IV}$ in the range [1.5, 4.5].

At $z < 1$, recent results based on *HST* UV data (Cooksey et al. 2009) give $\Omega_{\rm C\,IV} = (6 \pm 1) \times 10^{-8}$ corresponding to a 2.8 ± 0.5 increase over the $1.5 < z < 5$ values.

In this paper, we present a new measurement of $\Omega_{\rm C\,IV}$ in the redshift range [1.5, 4] based on a sample of 25 high-resolution, high signal-to-noise ratio (S/N) QSO spectra plus an additional sample of eight QSO spectra from the literature.

The rest of the paper is organized as follows. The data are presented in Section 2. In Section 3, the analysis is carried out with the computation of $\Omega_{\rm C\,IV}$. The results are discussed in Section 4. Throughout this paper, we assume $\Omega_{\rm m} = 0.26$, $\Omega_\Lambda = 0.74$ and $h \equiv H_0/(100\,{\rm km\,s^{-1}\,Mpc^{-1}}) = 0.72$.

2 OBSERVATIONAL DATA SAMPLE

The core of our sample is formed by the high-resolution, high S/N QSO spectra already described in Saitta et al. (2007) and D'Odorico et al. (2008). Most of them were obtained with the Ultraviolet and Visual Echelle Spectrograph (UVES) spectrograph (Dekker et al. 2000) at the Kueyen unit of the European Southern Observatory (ESO) VLT (Cerro Paranal, Chile) in the framework of the ESO Large Programme (LP): 'The Cosmic Evolution of the IGM' (Bergeron et al. 2004).

In this work, three more QSOs were added to that sample, mainly to increase the redshift extension above $z \sim 3$. UVES spectra of the QSO, Q0055-269, PKS 2000−330 and PKS 1937−101, were downloaded from the ESO Archive and reduced with the UVES pipeline following the standard procedure. The continuum level

⋆Based on observations collected at the European Southern Observatory Very Large Telescope, Cerro Paranal, Chile – Programs 166.A-0106(A), 65.O-0296(A) – and during commissioning and science verification of UVES.

†E-mail: dodorico@oats.inaf.it

Table 1. Relevant properties of the QSOs forming the total sample (see text for further details).

QSO	z_{em}	$\Delta z_{C\,IV}$
HE 1341-1020	2.142	1.467–2.090
Q0122-380	2.2004	1.513–2.147
PKS 1448−232	2.224	1.531–2.171
PKS 0237−23	2.233	1.538–2.179
J2233-606	2.248	1.550–2.194
HE 0001-2340	2.265	1.564–2.211
HS 1626+6433[a]	2.32	1.607–2.265
HE 1122-1648	2.40	1.665–2.344
Q0109-3518	2.4057	1.674–2.349
HE 2217-2818	2.414	1.681–2.357
Q0329-385	2.435	1.697–2.378
HE 1158-1843	2.448	1.707–2.391
HE 1347-2457	2.5986	1.826–2.539
Q1442+2931[a]	2.661	1.875–2.600
Q0453−423	2.669	1.881–2.608
PKS 0329−255	2.696	1.902–2.635
HE 0151-4326	2.763	1.955–2.701
Q0002-422	2.769	1.959–2.707
HE 2347-4342	2.880	2.067–2.816
SBS 1107+487[a]	2.966	2.114–2.900
HS 1946+7658	3.058	2.181–2.991
HE 0940-1050	3.0932	2.214–3.025
Q0420-388	3.1257	2.239–3.057
S4 0636+68[a]	3.175	2.278–3.106
SBS 1425+606[a]	3.199	2.297–3.129
PKS 2126−158	3.292	2.370–3.221
B1422+231	3.623	2.630–3.546
Q0055-269	3.66	2.659–3.583
PKS 2000−330	3.783	2.756–3.704
PKS 1937−101	3.787	2.770–3.400
PSS J1646+5514[a]	4.059	2.972–3.975
PSS J1057+4555[a]	4.131	3.029–4.046
BR 2237-0607[a]	4.559	3.365–4.467

[a]QSOs from BSR03.

was determined by interpolating with a cubic spline of the region of the spectrum free from evident absorption features.

For all the QSO in the sample (see Table 1), the C IV forest was defined as the interval between the Lyα emission and 5000 km s^{-1} from the C IV emission to avoid the proximity region where most of the intrinsic systems are found. The absorption features present in this wavelength interval were identified by inspecting the spectra by eye to look for the most common doublets (C IV, Mg II and Si IV). Then, other lines were identified testing their compatibility with the C IV, Mg II and Si IV redshifts. Finally, lines whose identity was still unknown after this operation were associated with metal systems detected in the Lyα forest or recognized as part of other multiplets (e.g. Fe II).

The C IV doublets were fitted with Voigt profiles using the LYMAN context of the MIDAS reduction package (Fontana & Ballester 1995). A minimum number of components were adopted to fit the velocity profile in order to reach a normalized $\chi^2 \sim 1$. The fit parameters for all the detected C IV lines are reported in Table 2.[1] In the following, we will refer to C IV *components* or simply C IV *lines* meaning the velocity components in which every absorption profile has been decomposed. However, in order to compare our results with previous works and with data at lower resolution, we will work also with C IV *systems* formed by groups of components. C IV *systems* were defined in the following way: for each list of C IV components corresponding to a single QSO, the velocity separations among all the lines have been computed and sorted in ascending order. If the smallest separation is less than $dv_{min} = 50$ km s^{-1} (corresponding to the velocity separation adopted by S01), the two lines are merged into a new line with column density equal to the sum of the column densities, and redshift equal to the average of the redshifts weighted with the column densities of the components. The velocity separations are then computed again and the procedure is iterated till the smallest separation becomes larger than dv_{min}.

[1] Only a sample is included here; the complete tables are available with the electronic version of the article (see Supporting Information).

Table 2. C IV absorption lines: HE 1341-1020 ($z_{em} = 2.142$)

z	b (km s^{-1})	log N(C IV)
1.699 561	15.4 ± 0.7	13.44 ± 0.03
1.699 690	5.7 ± 0.3	13.68 ± 0.02
1.699 818	10.3 ± 0.6	13.54 ± 0.03
1.700 051	7.3 ± 0.6	12.87 ± 0.04
1.700 284	18.9 ± 1.6	13.07 ± 0.03
1.700 996	13.9 ± 1.2	13.04 ± 0.07
1.700 812	29.6 ± 2.5	13.00 ± 0.08
1.701 957	6.9 ± 0.3	12.71 ± 0.01
1.703 648	9.5 ± 0.4	12.78 ± 0.01
1.854 894	10.2 ± 1.0	12.39 ± 0.03
1.910 582	7.5 ± 0.5	12.54 ± 0.02
1.910 986	13.7 ± 1.8	12.33 ± 0.05
1.911 525	3.9 ± 1.5	11.88 ± 0.07
1.914 971	9.6 ± 1.7	12.16 ± 0.08
1.915 286	16.2 ± 1.8	12.99 ± 0.04
1.915 507	9.2 ± 0.8	12.75 ± 0.06
1.998 137	6.9 ± 0.7	12.20 ± 0.03
2.041 423	9.1 ± 0.4	13.06 ± 0.03
2.041 588	9.9 ± 0.9	12.80 ± 0.06
2.084 978	10.5 ± 0.3	12.88 ± 0.01

Our sample consists of 1023 C IV velocity components with column densities $10^{12} \lesssim N(\mathrm{C\,IV}) \lesssim 10^{15}$ cm^{-2} and of 508 C IV systems in the same column density range.

The C IV absorptions in the spectra of 19 of the QSOs forming our sample were already identified and fitted by Scannapieco et al. (2006), using the software package VPFIT.[2] We refer to that paper for a careful analysis of the clustering properties of C IV lines and a comparison with the properties of Si IV, Mg II and Fe II lines. Unfortunately, the authors did not publish the individual Voigt parameters of their fitting.

2.1 Additional data sample

In order to further increase the number of C IV lines and to extend the sample to higher redshift, we have considered the C IV lines fitted in nine QSO spectra observed with High Resolution Echelle Spectrometer (HIRES) at Keck at a resolution and S/N similar to those of our spectra and reported in BSR03. The fit with Voigt profiles was carried out by the authors with VPFIT. The main difference between LYMAN and VPFIT is that the number of components fitted to a given velocity profile is, in general, larger using the latter (see also the discussion in Saitta et al. 2007). This is also seen in the present

[2] http://www.ast.cam.ac.uk/∼rfc/vpfit.html

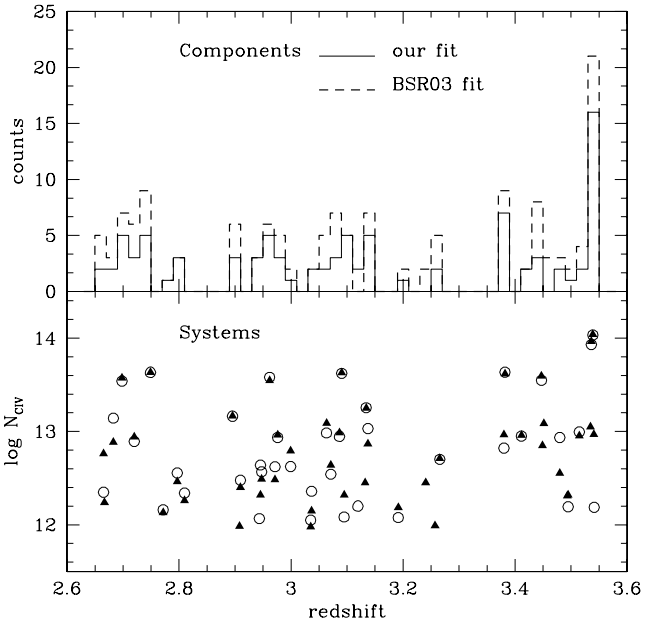

Figure 1. Upper panel: number of components of the C IV absorption systems in the spectrum of B1422+231 as fitted by us (solid line) and by BSR03 (dashed line). Lower panel: column densities of the C IV systems of B1422+231 computed by us (open dots) and by BSR03 (solid triangles).

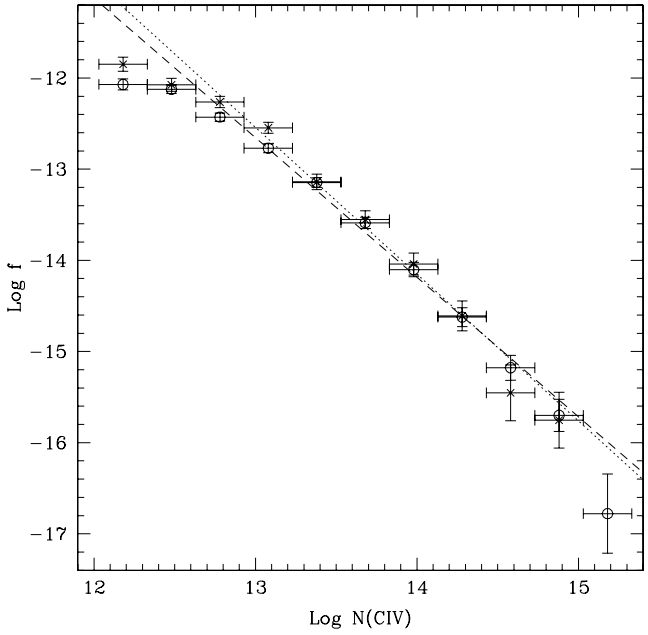

Figure 2. Comparison of the column density distribution function of C IV systems for Sample A (open dots) and Sample B (crosses) in the common redshift range $1.6 < z < 3.6$. The bin-size is $10^{0.3}$ $N(\mathrm{C\,IV})\,\mathrm{cm}^{-2}$ and the error bars are $\pm 1\,\sigma$, based on the number of points in each bin. The dashed and dotted lines are power laws of the form $f(N) = BN^{-\alpha}$ with index $\alpha =$ 1.53 and 1.71, respectively (see text).

case, in particular from the comparison of the C IV lines detected in the spectrum of the QSO B1422+231, which is the only object in common between the two samples. We find that in all cases, the number of components found with VPFIT is larger or equal to that found with LYMAN. However, when the total column density of each absorption system is considered, the difference between the two fitting procedures becomes negligible.

This is shown in Fig. 1 where the number of C IV components (upper panel) and the total column density of C IV systems (lower panel) obtained with the two fitting packages are compared. While the number of components is significantly larger in the fit by BSR03, the total column densities are most of the time in very good agreement.

The sample of BSR03 is formed by 577 C IV components and 302 C IV systems in the column density range $10^{12} \lesssim N(\mathrm{C\,IV}) \lesssim 10^{15}\,\mathrm{cm}^{-2}$. In the following, we will refer to our sample of C IV lines as *Sample A* and to the BSR03 sample as *Sample B* (excluding the lines of B1422+231, which are already in Sample A). The *total sample* is the sum of Sample A and Sample B. All the QSOs forming this sample are reported in Table 1 with their emission redshift and the redshift range covered by the C IV forest.

3 DATA ANALYSIS

3.1 The C IV column density distribution function, $f(N)$

$f(N)$ is extremely sensitive to the velocity decomposition of absorption features, since it is defined as the number of lines per unit column density and per unit redshift absorption path, dX (Tytler 1987). In the assumed cosmology, the redshift absorption path is

$$dX \equiv (1+z)^2[\Omega_{\mathrm{m}}(1+z)^3 + \Omega_\Lambda]^{-1/2}\,\mathrm{d}z. \quad (1)$$

In order to compare with the previous works, $f(N)$ has been computed for the C IV systems in Samples A and B in the common redshift interval, $1.6 < z < 3.6$ (see Fig. 2). The excess of low column density systems in BSR03 is due to their overdecomposition of the C IV velocity profiles with respect to our fit. A maximum-likelihood fit to the data with column densities $\log N(\mathrm{C\,IV}) \geq 13$ (binned in Fig. 2 for display purposes only) to a power law of the form $f(N) = BN^{-\alpha}$ gives an index $\alpha = 1.71 \pm 0.07$ for Sample A and $\alpha = 1.8 \pm 0.1$ for Sample B. Both are in agreement with the result by S01 based on C IV systems defined in the same way. These are steeper than the Ellison et al. (2000) fit of 1.44 ± 0.05 based on the very high SNR spectrum of B1422+231 and extending the power law down to $\log N(\mathrm{C\,IV}) \sim 12.3$.

In order to estimate the incompleteness of our data for $\log N(\mathrm{C\,IV}) \leq 13$, we have performed the following simulations. Four fake C IV doublets have been generated for each spectrum in our sample, with column densities $12 \leq N(\mathrm{C\,IV}) \leq 13$ and redshift chosen randomly from the redshift ranges reported in Table 1. The b-values of the fake C IV lines were drawn at random from the observed distribution of b-values in our data. These fake C IV doublets were then added to the real spectra and searched for by the member of our team who had previously identified the real C IV lines. Given the visual, rather than automatic, character of our searches, only two such trials were performed. The results of these tests are collected in Table 3.

We found that we could recover essentially all C IV doublets as long as $\log N(\mathrm{C\,IV}) \geq 12.6$. For $\log N(\mathrm{C\,IV}) = 12.3$, a correction

Table 3. Results of incompleteness tests.

$\log N(\mathrm{C\,IV})$	Fraction of detected C IV
12.00	0.60
12.30	0.82
12.60	0.97
12.78	0.97
13.00	1.00

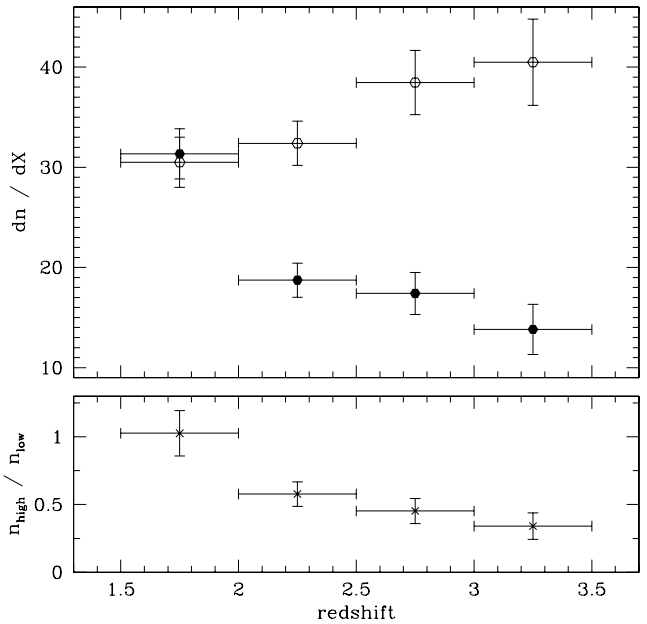

Figure 3. Upper panel: redshift evolution of the number density of the C IV lines in Sample A divided into low column density [open dots, $12 \leq \log N(\mathrm{C\,IV}) \leq 13$] and high column density [solid dots, $13 < \log N(\mathrm{C\,IV}) \leq 15$] absorptions. Lower panel: redshift evolution of the ratio between the number of high and low column density C IV lines.

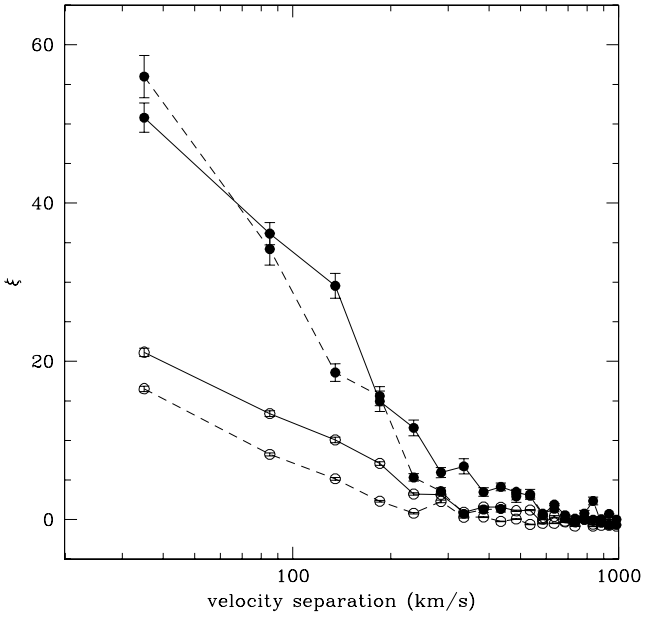

Figure 4. Two-point correlation function of the C IV lines in Sample A divided into low column density [open dots, $12 \leq \log N(\mathrm{C\,IV}) \leq 13$] and high column density [solid dots, $13 < \log N(\mathrm{C\,IV}) \leq 15$] absorptions. Solid lines trace the result for the redshift bin $1.5 \leq z \leq 2.3$ while dashed lines refer to the bin $2.3 < z \leq 3.5$.

factor of 1.2 has been determined (31/38 fake C IV systems detected in the incompleteness tests). In the lowest column density bin, $\log N(\mathrm{C\,IV}) = 12$, 24 over 40 C IV lines have been identified, corresponding to a correction factor of 1.7. The average Doppler parameter of the undetected C IV lines is $\langle b \rangle \sim 17.5$ km s^{-1}, while detected lines have $\langle b \rangle \sim 9$ km s^{-1}.

Extending the range of fitted data to our completeness limit, $\log N(\mathrm{C\,IV}) \geq 12.6$, the maximum-likelihood indexes become $\alpha = 1.53 \pm 0.04$ for Sample A and $\alpha = 1.61 \pm 0.07$ for Sample B, in agreement with the result by Ellison et al. (2000). If the correction factors reported above are applied to the points of Sample A, their values increase slightly to coincide with the values in Sample B shown in Fig. 2. The corrected value of the lowest column density bin is still too low to be fitted with the previously derived power laws.

3.2 The number density of C IV lines, d*n*/d*X*

The evolution with redshift of $\mathrm{d}n/\mathrm{d}X$ computed for C IV lines in Sample A is reported in the upper panel of Fig. 3. In particular, we have split our sample into weak and strong lines characterized by column densities $12 \leq \log N(\mathrm{C\,IV}) \leq 13$ and $13 < \log N(\mathrm{C\,IV}) \leq 15$, respectively. The two populations show different behaviours, with the weak lines being consistent with no evolution and the strong ones significantly decreasing in number towards higher redshifts. The latter trend confirms the result by Steidel (2009). Furthermore, the ratio of the number of strong and weak lines shows a steady decrease with redshift.

3.3 The two-point correlation function of C IV lines, *ξ(v, v + Δv)*

We computed $\xi(v, v + \Delta v)$ for the weak and strong C IV components and for two redshift intervals $1.5 < z < 2.3$ and $2.3 < z < 3.5$ (see Fig. 4). The obtained two-point correlation functions show a characteristic clustering scale r_0 (in redshift space) for the sample at high column densities, which is about 1.5–2 times larger than for the low column density lines (∼850 versus 500 km s^{-1} in the high-redshift bin and 700 versus 314 km s^{-1} for the low-redshift bin, with 1σ errors of about 150 km s^{-1}). Converting these scales into comoving Mpc h^{-1} at a given redshift, it appears that the low column density sample has clustering properties similar to those of Lyman-break galaxies (LBGs) at $z \sim 3$ (e.g. Porciani & Giavalisco 2002), while large column density C IV systems are more strongly clustered and possibly sample denser environment and more massive objects. Adelberger et al. (2005) reached similar conclusions from the analysis of a large sample of LBGs observed in the fields of 23 high-redshift QSOs.

3.4 The redshift evolution of the mass density of C IV

We used our sample of absorption lines also to compute the mass density of C IV as a fraction of the critical density today:

$$\Omega_{\mathrm{C\,IV}} = \frac{H_0\, m_{\mathrm{C\,IV}}}{c\, \rho_{\mathrm{crit}}} \int N f(N)\, \mathrm{d}N, \tag{2}$$

where $H_0 = 100\,h$ km s^{-1} Mpc^{-1} is the Hubble constant, $m_{\mathrm{C\,IV}}$ is the mass of a C IV ion, c is the speed of light, $\rho_{\mathrm{crit}} = 1.88 \times 10^{-29}\, h^2$ g cm^{-3} and $f(N)$ is the Column Density Distribution Function (CDDF). Since $f(N)$ cannot be recovered correctly for all column densities due to incompleteness and poor statistics, the integral in equation (2) can be approximated by a sum:

$$\Omega_{\mathrm{C\,IV}} = \frac{H_0\, m_{\mathrm{C\,IV}}}{c\, \rho_{\mathrm{crit}}} \frac{\sum_i N_i(\mathrm{C\,IV})}{\Delta X}, \tag{3}$$

with an associated fractional variance:

$$\left(\frac{\delta \Omega_{\mathrm{C\,IV}}}{\Omega_{\mathrm{C\,IV}}}\right)^2 = \frac{\sum_i [N_i(\mathrm{C\,IV})]^2}{\left[\sum_i N_i(\mathrm{C\,IV})\right]^2} \tag{4}$$

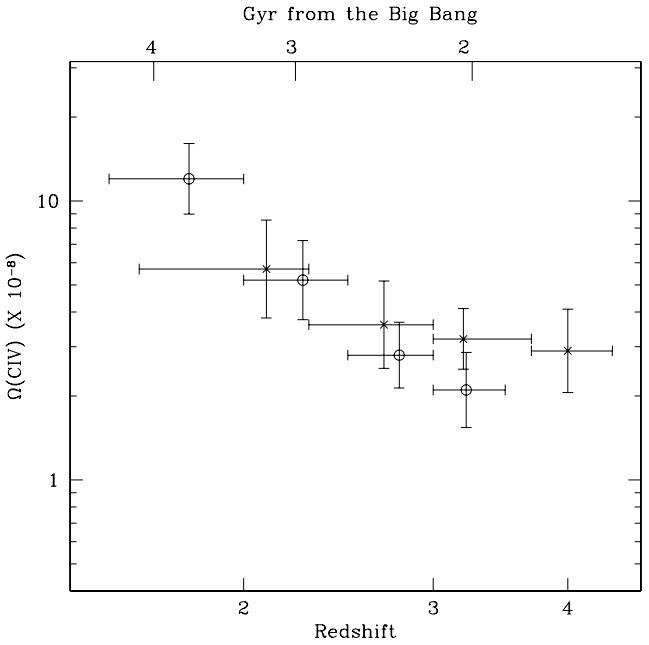

Figure 5. Comparison of the $\Omega_{\rm C\,IV}$ determinations based on C IV lines in Sample A (open dots) and the results by BSR03 (crosses). Error bars are 1σ.

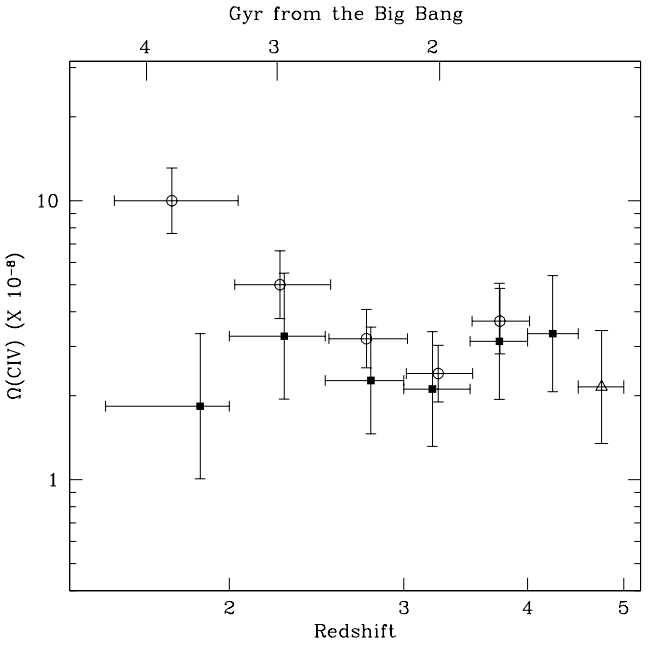

Figure 6. $\Omega_{\rm C\,IV}$ determined for the systems in the total sample (open dots) with 1σ error bars from bootstrap method compared with the results by S01 (solid squares) and by Pettini et al. (2003) (empty triangle).

as proposed by Storrie-Lombardi, McMahon & Irwin (1996). Error bars have been computed also using a bootstrap technique to build 1000 samples of QSO spectra, based on the observed sample, for each redshift bin and determining the standard deviation of the resulting distribution of $\Omega_{\rm C\,IV}$ values. This estimate is always slightly larger (by a factor of $\sim$1.5 or smaller) than the one based on equation (4) and has been used as the reference one.

The value of $\Omega_{\rm C\,IV}$ significantly depends on the column density range over which the sum or the integration is carried out, and as a consequence on the resolution and SNR of the available spectra. To take this aspect into account, we have computed three sets of values to be compared consistently with different data in the literature.

$\Omega_{\rm C\,IV}$ obtained for the C IV components in Sample A with column densities $12 \leq \log N({\rm C\,IV}) \leq 15$ is compared with the values reported in the original paper by BSR03 in Fig. 5. Our results confirm and strengthen the increasing trend with decreasing redshift of $\Omega_{\rm C\,IV}$, which was already present in the data by BSR03.

In order to carry out a comparison with the data set by S01, the most used in the literature for the redshift range [1.5, 4.5], $\Omega_{\rm C\,IV}$ has been computed from the C IV systems[3] of the total sample with column densities $12 \leq \log N({\rm C\,IV}) \leq 15$. In Fig. 6, these results are reported together with the value of S01 corrected for the assumed cosmology (they assumed Einstein–de Sitter) and with error bars derived from their plot and transformed to 1σ. The present data sample represents an increase in the absorption redshift path of a factor of 2.5 and 2 in the redshift bins [1.5, 2.0] and [2.0, 2.5], respectively, with respect to S01. Indeed, our estimate in the lowest redshift bin is $\sim 4.5\sigma$, larger than the previously accepted value, suggesting a trend of increasing C IV mass going to lower redshifts. The computed values with the associated errors are reported in Table 4.

[3] We remind the readers that C IV systems have been built adopting a minimum velocity separation of 50 km s^{-1} as reported in S01.

Table 4. $\Omega_{\rm C\,IV}$ for the systems in the total sample selected in the reported column density intervals.

z range	ΔX	Lines	$\Omega_{\rm C\,IV}$ ($\times 10^{-8}$)	$\delta\Omega$ ($\times 10^{-8}$)	$(\delta\Omega)_{\rm boot}$ ($\times 10^{-8}$)
$12 \leq \log N({\rm C\,IV}) \leq 15$					
1.5–2.0	16.61	148	10.0	1.8	2.7
2.0–2.5	28.11	211	5.0	1.0	1.4
2.5–3.0	19.82	161	3.2	0.7	0.8
3.0–3.5	13.91	132	2.4	0.4	0.6
3.5–4.0	7.60	78	3.7	0.7	1.0
$13.8 \leq \log N({\rm C\,IV}) \leq 15$					
1.5–2.1	22.56	41	6.5	1.3	1.9
2.1–2.5	22.16	23	4.4	1.2	1.7
2.5–3.0	19.85	19	2.8	0.8	0.9
3.0–4.0	21.50	17	1.3	0.3	0.4

We have not applied corrections to the values of $\Omega_{\rm C\,IV}$ due to the incompleteness of our observations for C IV lines with column densities $\lesssim$12.6, since we estimated them to be less than 3 per cent (less than 1 per cent in the lowest redshift bin). This is due to the small correction factors determined in Section 3.1 and to the small contribution of low column density lines to the final values.

Recently, the determinations of $\Omega_{\rm C\,IV}$ have been extended to very low ($z < 1$; e.g. Cooksey et al. 2009) and very high ($z > 5$; Becker et al. 2009; Ryan-Weber et al. 2009) redshift. Observations in these redshift ranges are more difficult since the C IV transition moves to the UV and to the IR region of the electromagnetic spectrum, respectively. As a consequence, the estimates of $\Omega_{\rm C\,IV}$ are based on lower resolution and lower SNR spectra, limiting the detectability of C IV lines to larger column densities. In order to study the evolution of $\Omega_{\rm C\,IV}$ in the whole redshift range between $z \sim 0$ and 6, we have carried out a third computation of the values of $\Omega_{\rm C\,IV}$ for C IV systems in the column density range $13.8 \leq \log N({\rm C\,IV}) \leq 15$, changing the

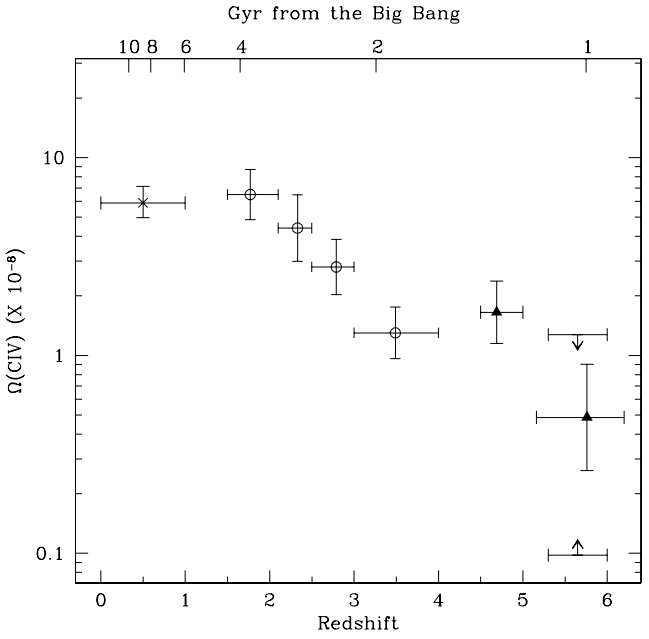

Figure 7. Estimates of $\Omega_{\rm C\,IV}$ in the redshift range $z \simeq 0$–6 for C IV systems with $13.8 \leq \log N({\rm C\,IV}) \leq 15$: cross (Cooksey et al. 2009); *open dots* total sample this work; *solid triangles* (Pettini et al. 2003 and Ryan-Weber et al. 2009); *95 per cent confidence interval* (Becker et al. 2009).

definition of the redshift bins in order to have comparable absorption redshift paths covered in each one of them. The column density lower boundary is the limit to which the higher (and lower) redshift surveys cited above are sensitive (being based on lower resolution and SNR spectra than those analysed in the present work). The results are shown in Fig. 7, where the point at $z \simeq 4.69$ is the determination by Pettini et al. (2003), corrected for the considered column density range by Ryan-Weber et al. (2009). The plot clearly shows the smooth growth of the value of $\Omega_{\rm C\,IV}$ from the plateau at redshifts 3–5 to the local value, corresponding to an increase of a factor of ∼5. Our determinations are also reported in Table 4.

4 DISCUSSION

In this paper, we have presented a new determination of the cosmological mass density of C IV, $\Omega_{\rm C\,IV}$, at $z = [1.5, 4]$ based on a large sample of high-resolution, high S/N QSO spectra, which more than doubles, with respect to previous measurements, the covered absorption path for $1.5 \lesssim z \lesssim 2.5$. The main result of our calculation is that $\Omega_{\rm C\,IV}$ is no longer approximately constant in the considered redshift range, but shows a steady increase from $z \sim 3$–5 to $z \sim 1.5$–2. On the other hand, it appears that the C IV mass density is not evolving significantly from these redshifts down to the present epoch (Cooksey et al. 2009).

The value of $\Omega_{\rm C\,IV}$ for the column density interval $12 \leq \log N({\rm C\,IV}) \leq 15$ can be converted into the IGM carbon content by mass, with the formula

$$Z_{\rm C} \simeq \frac{\Omega_{\rm C\,IV}}{\Omega_{\rm b}} \frac{\rm C}{\rm C\,IV} \qquad (5)$$

where $\Omega_{\rm b} = 0.0224/h^2$ (Pettini et al. 2008) is the contribution of baryons to the critical density and C IV/C is the fraction of C, which is triply ionized and depends on the assumed ionizing background. Assuming the maximum relative abundance of C IV, that is C IV/C $\lesssim$0.5, and the solar carbon over hydrogen abundance by mass $Z_{\rm C,\odot} = 0.0029$ (Asplund, Grevesse & Sauval 2005), we obtain a lower limit at redshifts [2.5, 4.0] of $Z_{\rm C} \gtrsim 1.4 \times 10^{-6} = 4.9 \times 10^{-4}\ Z_{\rm C,\odot}$ or [C/H] $\gtrsim -3.3$. At redshift [1.5, 2.0]: $Z_{\rm C} \gtrsim 4.6 \times 10^{-6} = 1.6 \times 10^{-3}\ Z_{\rm C,\odot}$ or [C/H] $\gtrsim -2.8$, corresponding to an increase of a factor of ∼3 with respect to the high-redshift bin.

The metallicity measured at high redshift is in agreement with the result obtained at $z = 3$ by Schaye et al. (2003) with the pixel optical depth method, in the case of overdensities above ∼10. This is consistent with the fact that $\Omega_{\rm C\,IV}$ traces mainly the metallicity of the overdense regions in the proximity of galaxies and its redshift evolution is linked with that of the strong systems. Simcoe, Sargent & Rauch (2004) found a median metallicity [C, O/H] $\simeq -2.8$ for the intergalactic gas at $z \sim 2.5$ with a method based on the direct detections of the absorption lines, which takes into account also the upper limits. Re-normalizing our result to the solar abundances and the fraction of C triply ionized adopted by those authors (C IV/C $\lesssim$ 0.25), we obtain [C/H] $\gtrsim -3.0$ consistent with their result.

The physical explanation for the redshift evolution of $\Omega_{\rm C\,IV}$ can be explored with cosmological simulations. We will devote a subsequent paper to the comparison between observations and predictions of hydrosimulations with a detailed treatment of metal enrichment (Tescari et al., in preparation). In the following, we will briefly discuss the few predictions of $\Omega_{\rm C\,IV}$ present in the literature and compare them with our results.

Oppenheimer & Davé (2006, hereafter OD06) have run cosmological hydrosimulations of galaxy formation meant to reproduce the metallicity of the IGM, where metals are expelled from galaxies by momentum-driven winds (whose velocity is proportional to the dispersion velocity of the galaxies). Those winds are very effective in transporting the gas without heating it too much. Their fiducial simulation consistently reproduces the star formation rate of the Universe, the volume-averaged metallicity of the IGM and the lack of evolution of $\Omega_{\rm C\,IV}$ from $z \approx 5 \rightarrow 1.5$, as observed in the data available at the time. On the other hand, the predicted mass density of C increases by nearly an order of magnitude towards lower redshifts in the same redshift interval, due to the increase in the total metallicity of the gas. The constant behaviour of $\Omega_{\rm C\,IV}$ is obtained by balancing the increase in C abundance with galactic winds. This form of feedback heats the IGM causing a decrease of the C IV ionization fraction. In particular, the peak of the C IV ionization fraction distribution as a function of overdensity shifts toward larger overdensities as redshift decreases. This is consistent with the increase in the ratio between strong and weak C IV systems at lower redshifts shown in Fig. 3 and the identification of strong systems with denser environment as deduced from the observed two-point correlation function (see Section 3.3).

To conclude, none of the models proposed by OD06 predicts an increase of $\Omega_{\rm C\,IV}$ towards lower redshifts. An improvement in the physics of the wind, plus the introduction of the AGB feedback, results in a slight increase of $\Omega_{\rm C\,IV}$ in the ranges $z < 0.5$ and $z > 5$ leaving the other values substantially unchanged (Oppenheimer & Davé 2008, hereafter OD08).

An effect which has not been taken into account up to now is the evolution in the shape of the UV background due to the He II re-ionization process expected at redshift ∼3. Naively, due to the increase in the number of free hard photons (ionizing C IV into C V) at the end of the re-ionization epoch, we would expect a trend opposite to what is observed: a decrease of the amount of C IV after $z \sim 3$. However, the details of this process are still under study (e.g. Bolton, Oh & Furlanetto 2009; Madau & Haardt 2009) and other factors should be accounted for properly: the decrease in the number density of QSOs going towards lower redshifts and the fact

that at low z the regions traced by the strong C IV absorbers (driving the evolution of $\Omega_{\rm C\,IV}$) could be only mildly affected by the cosmic UV background.

The observed rise of the cosmic C IV mass density in the redshift range 1.5–2.5 puts a strong constraint on the models describing the interplay between galaxies and their surrounding medium, suggesting that something is still missing in the physical implementation of galactic feedback.

ACKNOWLEDGMENTS

We would like to thank Eros Vanzella for his precious help in generating the synthetic C IV absorbers. We are grateful to the anonymous referee, whose comments and advice allowed us to improve this paper significantly. This research has been partially supported by ASI, Contract No. I/016/07/0 COFIS, INFN PD51 grant and PRIN MIUR. FC is supported by a fellowship by PRIN MIUR.

REFERENCES

Adelberger K. L., Shapley A. E., Steidel C. C., Pettini M., Erb D. K., Reddy N. A., 2005, ApJ, 629, 636
Asplund M., Grevesse N., Sauval A. J., 2005, in Barnes T. G. III, Bash F. N. eds, ASP Conf. Ser. Vol. 336, Cosmic Abundances as Records of Stellar Evolution and Nucleosynthesis. Astron. Soc. Pac., San Francisco, p. 25
Becker G. D., Rauch M., Sargent W. L. W., 2009, ApJ, 698, 1010
Bergeron J. et al., 2004, ESO The Messenger, 118, 40
Boksenberg A., Sargent W. L. W., Rauch M., 2003, preprint (astro-ph/0307557) (BSR03)
Bolton J. S., Oh S. P., Furlanetto S. R., 2009, MNRAS, 395, 736
Bunker A., Stanway E., Ellis R., McMahon R., Eyles L., Lacy M., 2006, New Astron. Rev., 50, 94
Cooksey K. L., Thom C., Prochaska J. X., Chen H.-W. 2009, ApJ, submitted (arXiv:0906.3347)
Dekker H., D'Odorico S., Kaufer A., Delabre B., Kotzlowski H., 2000, in Iye M., Moorwood A. F. M., eds, SPIE Proc. Vol. 4008, Optical and IR Telescope Instrumentation and Detectors. SPIE, Bellingham, p. 534
D'Odorico V., Bruscoli M., Saitta F., Fontanot F., Viel M., Cristiani S., Monaco P., 2008, MNRAS, 389, 1727
Ellison S. L., Songaila A., Schaye J., Pettini M., 2000, AJ, 120, 1175
Fontana A., Ballester P., 1995, ESO The Messenger, 80, 37
Madau P., Haardt F., 2009, ApJ, 693, L100
Oppenheimer B. D., Davé R., 2006, MNRAS, 373, 1265 (OD06)
Oppenheimer B. D., Davé R., 2008, MNRAS, 387, 577 (OD08)
Pettini M., Madau P., Bolte M., Prochaska J. X., Ellison S. L., Fan X., 2003, ApJ, 594, 695
Pettini M., Zych B. J., Murphy M. T., Lewis A., Steidel C. C., 2008, MNRAS, 391, 1499
Porciani C., Giavalisco M., 2002, ApJ, 565, 24
Ryan-Weber E. V., Pettini M., Madau P., 2006, MNRAS, 371, L78
Ryan-Weber E. V., Pettini M., Madau P., Berkeley J. Z., 2009, MNRAS, 395, 1476
Saitta F., D'Odorico V., Bruscoli M., Cristiani S., Monaco P., Viel M., 2008, MNRAS, 385, 519
Scannapieco E., Pichon C., Aracil B., Petitjean P., Thacker R. J., Pogosyan D., Bergeron J., Couchman H. M. P., 2006, MNRAS, 365, 615
Schaye J., Aguirre A., Kim T.-S., Theuns T., Rauch M., Sargent W. L. W., 2003, ApJ, 596, 768
Simcoe R. A., 2006, ApJ, 653, 977
Simcoe R. A., Sargent W. L. W., Rauch M., 2004, ApJ, 606, 92
Songaila A., 2001, ApJ, 561, L153 (S01)
Steidel C. C., 1990, ApJS, 72, 1
Storrie-Lombardi L., McMahon R. G., Irwin M., 1996, MNRAS, 283, 79
Tytler D., 1987, ApJ, 321, 49

SUPPORTING INFORMATION

Additional Supporting Information may be found in the online version of this article:

Table 2. C IV absorption lines.

Please note: Wiley-Blackwell are not responsible for the content or functionality of any supporting materials supplied by the authors. Any queries (other than missing material) should be directed to the corresponding author for the article.

This paper has been typeset from a TEX/LATEX file prepared by the author.